

## Structure and Lamb shift of $2s_{1/2}$ - $2p_{3/2}$ levels in lithiumlike $\text{Th}^{87+}$ through neonlike $\text{Th}^{80+}$

P. Beiersdorfer, A. Osterheld, S. R. Elliott, M. H. Chen, D. Knapp, and K. Reed  
*Lawrence Livermore National Laboratory, University of California, Livermore, California, 94551*  
 (Received 21 April 1995)

We report the measurement of thirteen  $2s_{1/2}$ - $2p_{3/2}$  dipole-allowed transitions in the highly ionized thorium ions  $\text{Th}^{80+}$  through  $\text{Th}^{87+}$ . The transitions have been measured with a high-resolution crystal spectrometer on the Livermore electron beam ion trap in which highly charged thorium ions were produced and excited in the interaction with a 100-keV electron beam. The observed  $2s_{1/2}$ - $2p_{3/2}$  transitions are readily identified from a qualitative analysis of the dipole-allowed radiative decay channels. The identifications are confirmed by detailed modeling calculations of the line excitation processes, which account for all radiative processes, including radiative cascades among levels in the  $n=2$  and  $n=3$  shells, and all electron-impact excitation processes. The transition energies have been determined with an overall accuracy of 35 ppm. A detailed discussion of the measurement uncertainties is given, including the effects of beam-induced polarization on the hydrogenic reference transitions used for calibration. Measurements of the  $1s^2$ - $1snp$  ( $n \leq 10$ ) transitions in heliumlike  $\text{Ar}^{16+}$ , which fall into the same wavelength region as the  $2s_{1/2}$ - $2p_{3/2}$  transitions in thorium, are presented that validate the estimate of our experimental uncertainties. These measurements achieved twice the accuracy of previous measurements of the  $\text{Ar}^{16+}$  lines. A value of  $4025.23 \pm 0.14$  eV is found for the  $2s_{1/2}$ - $2p_{3/2}$  transition in lithiumlike  $\text{Th}^{87+}$ . The value is sensitive to the effect of nuclear polarization and tests predictions of the 36-eV contribution from quantum electrodynamics to within 0.39%. A similar test of quantum electrodynamics calculations is given by the twelve  $2s_{1/2}$ - $2p_{3/2}$  transitions measured in the neighboring charge states. A comparison of the measured energies of the  $2s_{1/2}$ - $2p_{3/2}$  transitions in berylliumlike  $\text{Th}^{86+}$  through neonlike  $\text{Th}^{80+}$  with theoretical predictions from multiconfiguration Dirac-Fock calculations demonstrates the need for a better treatment of the electron-correlation terms in these highly charged multielectron ions. The measurements thus provide benchmarks for the development of theoretical approaches, such as relativistic many-body perturbation theory and large-scale configuration-interaction calculations, that attempt to account for electron correlations in very highly charged ions.

PACS number(s): 32.30.Rj, 12.20.Fv, 31.30.Jv

### I. INTRODUCTION

Contributions from quantum electrodynamics (QED) to atomic energy levels increase with higher powers of the nuclear charge  $Z$  than the Dirac energies. The effects of QED thus are enhanced in the spectra of the heaviest elements, and precise measurements can provide a very sensitive test of QED theory in intense nuclear fields. Such tests complement the many existing tests of QED in weak fields, which include measurements of the lepton anomalous magnetic moment or the structure of neutral hydrogen and helium, by assessing the nonperturbative aspects of QED theory in the limit ( $Z\alpha \approx 1$ ). They also complement tests of QED theory involving muonic atoms. The self-energy is unimportant in muonic atoms, while it contributes the dominant part to the QED terms in electronic atoms.

To gain a fundamental understanding of QED in the high- $Z$  limit, it is necessary to calculate the QED terms contributing to a given atomic system from first principles. While this problem has been solved for hydrogenic ions [1–5], it still remains an outstanding problem for the general case of many-electron ions. A test of QED theory in the intense fields of heavy nuclei is provided by measurements of  $K$ -shell transitions in neutral, heavy elements. For example, the 95-keV  $K\alpha_2$  transition in neutral uranium has been measured with a precision of 0.56 eV [6]. Agreement with calculations, which considered the screening effects of 91 electrons and included about 250 eV from QED, has been achieved within 5.4 eV [7,8]. The QED contributions in this

calculation, however, have not been computed from first principles. Instead, they were estimated from a scaling of the accurately known hydrogenic values through a plausible, but nevertheless phenomenological, prescription. The comparison with theory thus does not test the bound-state QED formalism itself but, strictly speaking, provides only a test of a theoretical approximation scheme tuned to account for the screening effects of inner and outer shell electrons. The comparison is also complicated experimentally by the presence of satellite transitions blending with the  $K\alpha$  transitions as well as by possible line shifts caused by chemical bonds when solid target material is used in the measurement.

In recent years, much progress has been made in performing *ab initio* calculations of the QED contributions to the energy levels in alkali-metal-like ions [9–13]. Alkali-metal-like ions are atomic systems with a single valence electron outside a closed shell and are thus most similar to the hydrogenic system. For such ions, it is now possible to evaluate radiative corrections using a rigorous formalism based on realistic atomic potentials. Moreover, the nonradiative energies can be calculated with very high precision for such systems, for example by using relativistic many-body perturbation theory (RMBPT) [14–17]. As a result, radiative and nonradiative terms can be isolated from each other and the result can be directly compared with experiments. This procedure allows a definitive experimental test of the bound-state QED formalism for single-valence-electron ions.

Efforts are currently under way to calculate the Dirac and

QED energies of systems with more than one valence electron and to achieve a precision similar to that attained for the alkali-metal-like ions, and much progress has been made [18,19]. To guide the development of such calculations, sufficiently precise measurements of the energy levels in very highly charged ions are needed that serve as benchmarks against which calculations can be checked.

The capability of producing and studying very highly charged very high- $Z$  ions in heavy-ion accelerator facilities was demonstrated in a measurement of the lifetime of the  $1s2p\ ^3P_0$  level in heliumlike  $U^{90+}$  by Munger and Gould [20]. The lifetime measurement was used to infer a  $260.0 \pm 7.9$ -eV energy difference with the  $1s2s\ ^3S_1$  level. Four additional accelerator-based measurements involving nearly bare uranium ions have since been reported. In the first, Schweppe *et al.* used a Doppler-tuned spectrometer to determine a  $280.59 \pm 0.10$ -eV splitting of the  $1s^22s\ ^2S_{1/2} - 1s^22p\ ^2P_{1/2}$  levels in lithiumlike  $U^{89+}$  [21]. Three other measurements focused on hydrogenic  $U^{91+}$  [22–24]. For example, Briand *et al.* determined a value of  $102\,313 \pm 120$  eV for the energy of the  $1s_{1/2} - 2p_{3/2}$  transition of hydrogenlike  $U^{91+}$  [22], while Stöhlker *et al.* and Lupton *et al.* subsequently determined  $102\,209 \pm 63$  eV and  $102\,130 \pm 92$  eV, respectively [23,24].

Another technique for producing and studying nearly bare uranium ions was recently demonstrated in a measurement of the splitting of the  $1s^22s\ ^2S_{1/2} - 1s^22p\ ^2P_{3/2}$  levels in lithiumlike  $U^{89+}$  [25]. The splitting was determined to be  $4459.37 \pm 0.35$  eV at a 90% confidence level (or  $4459.37 \pm 0.21$  eV at a 68% confidence level [26]). This measurement was carried out on a high-energy electron beam ion trap (EBIT). In this device stripping and excitation takes place in the interaction of trapped, stationary ions with a monoenergetic electron beam [27]. The mode of operation is thus the inverse of the beam-foil or beam-gas jet techniques used on heavy-ion accelerators. In these devices, the ions move at relativistic speeds and the electrons are at rest in the target. Because the ions trapped in EBIT are stationary, spectroscopic measurements are unaffected by Doppler shifts and standard spectroscopic techniques can be applied. As a result, it was possible to measure a total of thirteen  $2s_{1/2} - 2p_{3/2}$  electric-dipole transitions in the eight ionization stages  $U^{82+}$  through  $U^{89+}$  in a single experiment [25]. Thus, instead of providing information on a transition in a single charge state, as has been customary in Doppler-tuned or lifetime-based accelerator experiments, atomic-structure theory could be tested along a wide range of the isonuclear sequence.

In the following we apply the techniques developed in Ref. [25] to the study of the second-heaviest naturally occurring element. Specifically, we report a measurement of thirteen  $2s_{1/2} - 2p_{3/2}$  electric-dipole transitions in the eight adjacent charge states  $Th^{87+}$  through  $Th^{80+}$ . The measurements include the  $2s_{1/2} - 2p_{3/2}$  transition in lithiumlike  $Th^{87+}$ , whose transition energy is determined to be  $4025.23 \pm 0.14$  eV at the  $1\sigma$  confidence level or  $4025.23 \pm 0.19$  eV at the  $2\sigma$  confidence level. The present measurements achieved a significantly higher precision than the analogous measurement for uranium. The higher precision is the result of two factors. First, the energies of the thorium transitions were about 10% lower than those in uranium, increasing the resolving power of our spectrometer and thus the accuracy of the measure-

ments by a similar amount. Second and most importantly, improvements in the operation of the high-energy electron-beam ion trap enabled us to attain a significantly higher abundance of higher ionization states. In fact, charge states as high as bare uranium have now been achieved [28]. This improves the fraction of ions in the lithiumlike charge state and allows the collection of spectra with higher signal-to-noise ratios than obtained previously.

Our measurements of the  $2s_{1/2} - 2p_{3/2}$  transitions in highly charged thorium ions confirm the results obtained in the case of uranium. This is important, since no other measurements of the  $2s_{1/2} - 2p_{3/2}$  transitions are available for such very high- $Z$  ions. For example, apart from the recent measurement of uranium, the highest- $Z$  measurement among the lithiumlike  $2s_{1/2} - 2p_{3/2}$  transitions is the measurement of xenon [29]. In the case of the fluorinelike transitions, the highest- $Z$  measurement is that of antimony ( $Z=51$ ) [30], in the case of the oxygenlike transitions, it is that of tin ( $Z=50$ ) [30].

The paper is structured as follows. A discussion of the  $n=2$  level structure of all ionization stages between neonlike and lithiumlike thorium is given in the next section. Here, we delineate the transitions we expect to see in our measurements based upon the transitions possible among all excited  $n=2$  levels in a given charge state. We confirm our predictions with detailed modeling calculations, which are also presented in Sec. II. In Sec. III we discuss the production of highly charged thorium ions in the Livermore high-energy EBIT. The spectroscopic setup for analyzing the x-ray emission from the thorium ions is described in Sec. IV. A detailed discussion of the wavelength calibrations and experimental uncertainties is given in Sec. V. This includes a discussion of the various systematic uncertainties affecting our measurements, such as detector linearity and polarization effects on the position of the calibration lines. We present a test of the accuracy of our experimental technique by comparing the energies of  $1snp\ ^1P_1 \rightarrow 1s^2\ ^1S_0$  ( $5 \leq n \leq 10$ ) transitions in heliumlike  $Ar^{16+}$  with theoretical predictions. These transitions were measured using the same calibration lines and techniques as the thorium lines. In Sec. VI we compare the measured energies of the thorium transitions with those calculated with by various authors. Excellent agreement between the calculations of Blundell [13] and our measurement is found for the energy of the transition in lithiumlike  $Th^{87+}$ . By contrast, a comparison with results from multi-configurational Dirac-Fock (MCDF) calculations shows systematic discrepancies for each charge state. We summarize and conclude our discussion in Sec. VII.

## II. STRUCTURE OF THE $n=2$ CONFIGURATIONS AND PREDICTED LINE INTENSITIES

Because of the distinct groupings of the  $n=2 \rightarrow 2$  transitions and the fact that the excitation in EBIT takes place in the low-collisional limit, while at the same time dielectronic recombination involving only  $L$ -shell electrons is energetically forbidden and thus is nonexistent, it is relatively simple to understand the  $2s_{1/2} - 2p_{3/2}$  emission from highly charged thorium ions. In the following, we enumerate the features we expect to observe in the spectrum based on an analysis of the level configurations. Such an analysis predicts all strong

transitions observed in the spectrum, and it serves to elucidate the processes producing the line emission in an intuitive way. We have also performed detailed calculations of the spectral line intensities based on a collisional-radiative model. The results of these calculations validate and quantify our qualitative analysis. These results are presented at the end of this section.

### A. Level structure

Relativity and the spin-orbit interaction dominate the intrashell structure of highly charged high- $Z$  ions. The energy of an electron in the  $n=2$  shell differs by about 3.8 keV, depending on whether its total angular momentum is  $j=\frac{1}{2}$  or  $j=\frac{3}{2}$ . As a result, the energy of the  $2p_{3/2}\rightarrow 2s_{1/2}$  transition in lithiumlike  $\text{Th}^{87+}$  near 4.0 keV is very distinct from that of the  $2p_{1/2}\rightarrow 2s_{1/2}$  transition near 0.3 keV. Adding an additional electron to the  $n=2$  shell changes the overall transition energy typically by less than 1%. Consequently, all  $2p_{3/2}\rightarrow 2s_{1/2}$  transitions from the eight charge states lithiumlike through neonlike thorium fall within a narrow range of energy, i.e., within 4.0 and 4.2 keV, and thus are well resolved from the  $2p_{1/2}\rightarrow 2s_{1/2}$  transitions, which fall into the energy band 0.3–0.6 keV. Moreover, they are also well resolved from any possible  $2p_{3/2}\rightarrow 2p_{1/2}$  magnetic-dipole transitions. The energies of the latter transitions are about 0.3–0.6 keV lower than those of the  $2p_{1/2}\rightarrow 2s_{1/2}$  transitions because of a correspondingly higher energy of the  $2p_{1/2}$  electron compared to the  $2s_{1/2}$  electron. Hence, the possible  $2p_{3/2}\rightarrow 2p_{1/2}$  transitions fall into the energy band 3.5–3.7 keV in the case of thorium.

### B. Spectral contributions from $\Delta n=0$ excitations

The radiative decay rates of  $n=2\rightarrow 2$  transitions in the highly charged thorium ions are typically no less than about  $10^{10}\text{ s}^{-1}$  for magnetic-dipole and  $10^{14}\text{ s}^{-1}$  for electric-dipole transitions. These fast rates contrast starkly with the smallness of the electron-impact excitation cross sections for these highly charged ions. The electron-impact excitation cross sections range from about  $10^{-26}$  to  $10^{-23}\text{ cm}^2$  for 100-keV electrons. Since the electron density in EBIT is no more than about  $10^{12}\text{ cm}^{-3}$ , it is appropriate to assume that electron-impact excitation takes place in the low-collisional limit, i.e., that all excitations proceed from the ground state and are followed by radiative decay until they are again back in the ground state. In this case, it is relatively simple to enumerate all levels with valence electrons in the  $n=2$  shell that might contribute to the  $2p_{3/2}\rightarrow 2s_{1/2}$  spectrum in the 4.0–4.2-keV range.

The assumption of low collisionality requires the excitation of a  $2s_{1/2}$  electron from the ground state to fill a  $2p_{3/2}$  state and subsequent decay of a  $2p_{3/2}$  electron back to the  $2s_{1/2}$  vacancy in order to produce a  $2s_{1/2}$ - $2p_{3/2}$  transition. In the case of lithiumlike  $\text{Th}^{87+}$ , only the level  $1s^2 2p_{3/2}$  can be excited from the  $1s^2 2s_{1/2}$  ground state to produce exactly one  $2p_{3/2}\rightarrow 2s_{1/2}$  transition. Starting with the  $1s^2 2s^2$  ground state in berylliumlike  $\text{Th}^{86+}$ , two levels can be produced by exciting a  $2s_{1/2}$  electron. These are the levels  $(1s^2 2s_{1/2} 2p_{3/2})_{J=1}$  and  $(1s^2 2s_{1/2} 2p_{3/2})_{J=2}$ . Only the first is allowed by selection rules to contribute to the  $2p_{3/2}\rightarrow 2s_{1/2}$  spectrum. The second level is dipole-forbidden to decay to

the ground level. It decays instead via a  $2p_{3/2}\rightarrow 2p_{1/2}$  magnetic-dipole transition with a predicted branching ratio of more than 0.99. Similarly, the  $(1s^2 2s^2 2p_{1/2}^2)_{J=0}$  ground state in carbonlike  $\text{Th}^{84+}$  can be excited to the two levels  $(2s^2 2s_{1/2} 2p_{1/2}^2 2p_{3/2})_{J=1}$  or  $(1s^2 2s_{1/2} 2p_{1/2}^2 2p_{3/2})_{J=2}$ . Again, only the former is allowed to contribute to the  $2p_{3/2}\rightarrow 2s_{1/2}$  spectrum. The situation in fluorinelike  $\text{Th}^{81+}$  is similar to the lithiumlike case in that only one level can be excited from the ground state, namely, the level  $(1s^2 2s_{1/2} 2p^6)_{J=1/2}$ , resulting in one possible  $2p_{3/2}\rightarrow 2s_{1/2}$  transition.

Unlike the lithiumlike, berylliumlike, carbonlike, and fluorinelike charge states, which each contribute only one  $2p_{3/2}\rightarrow 2s_{1/2}$  transition, the boronlike, nitrogenlike, and oxygenlike charge states each contribute several transitions to the spectrum. The boronlike  $(1s^2 2s^2 2p_{1/2})_{J=1/2}$  ground state can be excited to the levels  $(1s^2 2s_{1/2} 2p_{1/2} 2p_{3/2})_{J=1/2, 3/2, 5/2}$ . Of these only those with total angular momentum  $J=\frac{1}{2}$  or  $J=\frac{3}{2}$  can decay via a dipole-allowed  $2p_{3/2}\rightarrow 2s_{1/2}$  transition back to the ground state. The boronlike ion thus contributes two transitions to the  $2s_{1/2}$ - $2p_{3/2}$  spectrum. The nitrogenlike  $(1s^2 2s^2 2p_{1/2}^2 2p_{3/2})_{J=3/2}$  ground state can be excited to the three levels  $(1s^2 2s_{1/2} 2p_{1/2}^2 2p_{3/2}^2)_{J=1/2, 3/2, 5/2}$ . Each of these levels is allowed to decay back to the ground state via a  $2p_{3/2}\rightarrow 2s_{1/2}$  transition contributing a total of three transitions. Finally, the oxygenlike  $(1s^2 2s^2 2p_{1/2}^2 2p_{3/2}^2)_{J=2}$  ground state can be excited to two levels, the levels  $(1s^2 2s_{1/2} 2p_{1/2}^2 2p_{3/2}^3)_{J=1}$  and  $(1s^2 2s_{1/2} 2p_{1/2}^2 2p_{3/2}^3)_{J=2}$ , that can decay via three dipole-allowed  $2p_{3/2}\rightarrow 2s_{1/2}$  transitions to either the ground state or the  $(1s^2 2s^2 2p_{1/2}^2 2p_{3/2}^2)_{J=0}$  level, which is the second lowest level in the oxygenlike ion.

A total of twelve transitions can be excited by the above scheme in the seven charge states lithiumlike through fluorinelike thorium. Additional transitions may be excited, however, if the assumptions used above are somewhat relaxed. While a true collisionless limit assumes that each charge state has exactly one ground state, formed by the level with the lowest energy, this may not be true for the conditions prevalent in EBIT. For example, the lowest two levels in the oxygenlike ion are identical in their electron configurations and differ only by their total angular momentum. Radiative decay from the second lowest level (with  $J=0$ ) to the lowest (with  $J=2$ ) must proceed via an electric quadrupole transition. The radiative decay rate is a mere  $90\text{ s}^{-1}$ . This is so slow that a substantial fraction of all oxygenlike ions may be in the  $J=0$  level. However,  $2s_{1/2}\rightarrow 2p_{3/2}$  excitation from the  $(2s^2 2s^2 2p_{1/2}^2 2p_{3/2}^2)_{J=0}$  level populates the same upper levels as excitation from the  $(1s^2 2s^2 2p_{1/2}^2 2p_{3/2}^2)_{J=2}$  level. Thus no new transitions would be produced.

Another exception to the validity of the assumptions of the low-collisional limit can be found in the case of berylliumlike ions. Here, a second possible ground state is given by the level  $(1s^2 2s_{1/2} 2p_{1/2})_{J=0}$ . This level is the second lowest berylliumlike level. In the absence of a nuclear moment, as is the case in  $^{232}\text{Th}$ ,  $J=0\rightarrow 0$  transitions are strictly forbidden. Thus the level may only decay via magnetic-dipole, electric-dipole two-photon decay, which is a highly unlikely radiative decay. As a result, a substantial fraction of the berylliumlike ions may occupy this level. Unlike the case of oxygenlike ions,  $2s_{1/2}\rightarrow 2p_{3/2}$  excitation from the second ground level in berylliumlike ions produces a  $2p_{3/2}\rightarrow 2s_{1/2}$  transition

that cannot be produced by excitation from the  $1s^2 2s^2$  ground state. In particular, excitation of the  $(1s^2 2s_{1/2} 2p_{1/2})_{J=0}$  level populates the level  $(1s^2 2p_{1/2} 2p_{3/2})_{J=1}$ , which results in a transition that proceeds from the level  $(1s^2 2p_{1/2} 2p_{3/2})_{J=1}$  to the  $(1s^2 2s^2)_{J=0}$  ground state. This transition is well resolved from the transition produced by excitation of the  $(1s^2 2s^2)_{J=0}$  ground state. Thus, if there is a substantial fraction of the berylliumlike ions in the  $(1s^2 2s_{1/2} 2p_{1/2})_{J=0}$  level, a distinct signature will be observable in the spectrum. Observation of this transition would thus allow an estimate of the fraction of berylliumlike ions in the second ground-state level.

### C. Spectral contributions from $\Delta n = 1$ excitations

So far, we have only considered excitation of a  $2s_{1/2}$  electron to the  $2p_{3/2}$  level. This type of excitation is impossible in the case of neonlike ions where all  $2p_{3/2}$  levels are filled. To enable a  $2p_{3/2} \rightarrow 2s_{1/2}$  transition, we must consider excitation of a  $2s_{1/2}$  electron to the  $n=3$  shell. Based on an earlier analysis of neonlike  $\text{Ag}^{37+}$ , the most likely candidate level that would result in a strong  $2p_{3/2} \rightarrow 2s_{1/2}$  transition is the level  $(1s^2 2s_{1/2} 2p^6 3s_{1/2})_{J=0}$  [31]. Because  $J=0 \rightarrow J=0$  transitions are strictly forbidden, this level cannot decay via an  $n=3 \rightarrow 2$  transition but must decay via an  $n=2 \rightarrow 2$  transition. In the case of neonlike  $\text{Ag}^{37+}$ , the  $(1s^2 2s_{1/2} 2p^6 3s_{1/2})_{J=0}$  level was the sixth most likely level to be excited from the  $^1S_0$  neonlike ground state [31]. We can expect that excitation of this level is also probable in the case of neonlike  $\text{Th}^{80+}$ . Moreover, the level will be populated yet more strongly if we allow for a large abundance of sodiumlike ions. In this case, the  $(1s^2 2s_{1/2} 2p^6 3s_{1/2})_{J=0}$  level is produced by ionization of a  $2s$  electron from a sodiumlike ion. This process also populates the level  $(1s^2 2s_{1/2} 2p^6 3s_{1/2})_{J=1}$ , which can decay to the level  $(1s^2 2s^2 2p_{3/2} 3s_{1/2})_{J=1}$ , but predominantly decays to the level  $(1s^2 2s^2 2p_{3/2} 3s_{1/2})_{J=2}$ . Another level that may result in a  $2p_{3/2} \rightarrow 2s_{1/2}$  transition is the level  $(1s^2 2s_{1/2} 2p^6 3d_{5/2})_{J=2}$ . In the analysis of neonlike  $\text{Ag}^{37+}$  it was the fifth most likely level to be excited from the ground state [31]. The level, however, was observed to decay via an electric quadrupole transition to the ground state in many ions [32,33], and the intensity of any  $2p_{3/2} \rightarrow 2s_{1/2}$  transition depends on the branching ratio. The same holds true for  $2s_{1/2} \rightarrow 2p_{3/2}$  decay of the level  $(1s^2 2s_{1/2} 2p^6 3d_{3/2})_{J=2}$ .

Excitation of a  $2s_{1/2}$  electron to the  $n=3$  level can also result in a  $2p_{3/2} \rightarrow 2s_{1/2}$  transition in the case of nitrogenlike, oxygenlike, and fluorinelike ions. The  $n=3$  electron in this case acts only as a spectator. Moreover, it is conceivable that there are levels in neonlike ions, other than those already discussed, with a  $2s_{1/2}$  vacancy and a spectator electron in the  $M$  shell that result in  $2p_{3/2} \rightarrow 2s_{1/2}$  transitions. It is, however, beyond the scope of a simple enumeration to estimate which of the possible levels actually contributes significantly to the  $2p_{3/2} \rightarrow 2s_{1/2}$  spectrum. To predict the intensity of such transitions a detailed model calculation is needed.

### D. Calculated electric dipole line intensities

We have constructed a detailed excitation model for predicting the  $2p_{3/2} \rightarrow 2s_{1/2}$  line intensities from data generated

with the Hebrew University–Lawrence Livermore atomic structure computer codes (HULLAC) [34]. The model included all levels with an optical electron in the  $n=2$  or  $n=3$  shell for all charge states, lithiumlike through neonlike. The model accounted for all radiative processes, including radiative cascades, involving electric or magnetic dipole or quadrupole transitions and all electron-impact excitation processes. To predict the effects of radiative electron capture and of ionization, the model included radiative electron capture into the  $n=2$  and  $n=3$  shells and the ionization of  $n=2$  electrons. This links a given ion species to its neighboring ion species. Thus, for correctly modeling the intensity of the lithiumlike and neonlike transitions, the ground-state levels of heliumlike and sodiumlike ions were added to the model.

The results of these model calculations validate the assumptions of low collisionality and confirm the existence of the lines predicted by considering electric-dipole decay among the possible level configurations. For all ionization stages except berylliumlike and oxygenlike ions, excitations proceed only from the ground state. Even in the case of berylliumlike and oxygenlike ions, only a small fraction of the total ion population is in the second-lowest level. In the case of berylliumlike  $\text{Th}^{86+}$ , the fraction of  $\text{Th}^{86+}$  ions in the level  $(1s^2 2s_{1/2} 2p_{1/2})_{J=0}$  is 7.6%; in the case of oxygenlike  $\text{Th}^{82+}$ , the fraction in the level  $(1s^2 2s^2 2p_{1/2}^2 2p_{3/2}^2)_{J=0}$  is 1.1%. This is so because electron collisions tend to excite levels that predominantly decay to the true ground state, bypassing secondary ground states.

Results from our collisional-radiative-model calculations for electron energies of 100 keV are presented in Table I. Because the model takes into consideration radiative capture into and ionization of neighboring charge states, the computed line intensities are (in some cases) sensitive to the assumed abundance of the various charge states. The results in Table I were obtained by assuming an equal abundance of all charge states. This is clearly incorrect, but the computed relative intensities in most cases do not depend strongly on this assumption. The only exceptions are some of the lines in neonlike thorium. As discussed earlier, the level  $(1s^2 2s_{1/2} 2p^6 3s_{1/2})_{J=1}$  is almost exclusively produced by ionization of sodiumlike ions. Transitions from this level will vanish, if no sodiumlike ions are present. Similarly, transitions from level  $(1s^2 2s_{1/2} 2p^6 3s_{1/2})_{J=0}$  will be reduced in intensity.

Table I shows that transitions with spectators in the  $n=3$  shell are prominent only in the case of neonlike ions. In the case of all other charge states where they are possible, such transitions are never stronger than about 3% of the strongest line. Also, the presence of the metastable level  $(2s_{1/2} 2p_{1/2})_{J=0}$  in berylliumlike thorium does not produce any strong transitions that are readily observable in the spectrum. The strongest of these lines has only 2.8% the intensity of the strongest line populated by electron-impact excitation of the true berylliumlike ground state.

## III. PRODUCTION OF HIGHLY CHARGED THORIUM IONS

The highly charged thorium ions were produced in the high-energy electron-beam ion trap (also dubbed SuperEBIT) at the Lawrence Livermore National Laboratory

TABLE I. Line intensities predicted by a detailed radiative-collisional model. The intensity of the strongest line in each charge state is set equal to 100.0 and lines with relative intensities as low as 1.0 are listed. For neonlike transitions, only lines larger than 10.0 are listed. Lines observed in the present measurement are labeled in the notation of Ref. [25].

Ion	Key	Transition	Relative intensity
Th <sup>87+</sup>	Li	$(2p_{3/2})_{J=3/2} \rightarrow (2s_{1/2})_{J=1/2}$	100.0
Th <sup>86+</sup>	Be	$(2s_{1/2}2p_{3/2})_{J=1} \rightarrow (2s^2)_{J=0}$	100.0
Th <sup>86+</sup>		$(2p_{1/2}2p_{3/2})_{J=1} \rightarrow (2s_{1/2}2p_{1/2})_{J=0}$	2.8
Th <sup>86+</sup>		$(2p_{1/2}2p_{3/2})_{J=1} \rightarrow (2s_{1/2}2p_{1/2})_{J=1}$	1.4
Th <sup>85+</sup>	B-1	$(2s_{1/2}2p_{1/2}2p_{3/2})_{J=3/2} \rightarrow (2s^22p_{1/2})_{J=1/2}$	100.0
Th <sup>85+</sup>	B-2	$(2s_{1/2}2p_{1/2}2p_{3/2})_{J=1/2} \rightarrow (2s^22p_{1/2})_{J=1/2}$	52.7
Th <sup>85+</sup>		$(2s_{1/2}2p_{1/2}2p_{3/2})_{J=3/2} \rightarrow (2s^22p_{1/2})_{J=1/2}$	3.3
Th <sup>84+</sup>	C	$(2s_{1/2}2p^22p_{3/2})_{J=1} \rightarrow (2s^22p^2)_{J=0}$	100.0
Th <sup>83+</sup>	N-3	$(2s_{1/2}2p^22p_{3/2}^2)_{J=3/2} \rightarrow (2s^22p^22p_{3/2})_{J=3/2}$	100.0
Th <sup>83+</sup>	N-1	$(2s_{1/2}2p^22p_{3/2}^2)_{J=5/2} \rightarrow (2s^22p^22p_{3/2})_{J=3/2}$	44.4
Th <sup>83+</sup>	N-2	$(2s_{1/2}2p^22p_{3/2}^2)_{J=1/2} \rightarrow (2s^22p^22p_{3/2})_{J=3/2}$	29.3
Th <sup>83+</sup>		$(2s_{1/2}2p^22p_{3/2}2s_{1/2})_{J=3/2} \rightarrow (2s^22p^23s_{1/2})_{J=3/2}$	1.3
Th <sup>82+</sup>	O-1	$(2s_{1/2}2p^22p_{3/2}^3)_{J=2} \rightarrow (2s^22p^22p_{3/2}^2)_{J=2}$	100.0
Th <sup>82+</sup>	O-3	$(2s_{1/2}2p^22p_{3/2}^3)_{J=1} \rightarrow (2s^22p^22p_{3/2}^2)_{J=2}$	60.5
Th <sup>82+</sup>	O-2	$(2s_{1/2}2p^22p_{3/2}^3)_{J=1} \rightarrow (2s^22p^22p_{3/2}^2)_{J=0}$	22.3
Th <sup>82+</sup>		$(2s_{1/2}2p^22p_{3/2}^23s_{1/2})_{J=2} \rightarrow (2s^22p^22p_{3/2}2s_{1/2})_{J=2}$	3.6
Th <sup>82+</sup>		$(2s_{1/2}2p^22p_{3/2}^23d_{5/2})_{J=4} \rightarrow (2s^22p^22p_{3/2}2d_{5/2})_{J=4}$	1.9
Th <sup>82+</sup>		$(2s_{1/2}2p^22p_{3/2}^23d_{3/2})_{J=4} \rightarrow (2s^22p^22p_{3/2}2d_{3/2})_{J=3}$	1.1
Th <sup>81+</sup>	F	$(2s_{1/2}2p^22p^4)_{J=1/2} \rightarrow (2s^22p^22p_{3/2}^3)_{J=3/2}$	100.0
Th <sup>81+</sup>		$(2s_{1/2}2p^22p_{3/2}^33s_{1/2})_{J=3/2} \rightarrow (2s^22p^22p_{3/2}^23s_{1/2})_{J=5/2}$	3.6
Th <sup>81+</sup>		$(2s_{1/2}2p^22p_{3/2}^33s_{1/2})_{J=3/2} \rightarrow (2s^22p^22p_{3/2}^23s_{1/2})_{J=1/2}$	1.7
Th <sup>81+</sup>		$(2s_{1/2}2p^22p_{3/2}^33d_{3/2})_{J=7/2} \rightarrow (2s^22p^22p_{3/2}^23d_{3/2})_{J=7/2}$	1.6
Th <sup>81+</sup>		$(2s_{1/2}2p^22p_{3/2}^33d_{5/2})_{J=7/2} \rightarrow (2s^22p^22p_{3/2}^23d_{5/2})_{J=9/2}$	1.4
Th <sup>81+</sup>		$(2s_{1/2}2p^22p_{3/2}^33s_{1/2})_{J=3/2} \rightarrow (2s^22p^22p_{3/2}^23s_{1/2})_{J=3/2}$	1.1
Th <sup>80+</sup>		$(2s_{1/2}2p^22p^43s_{1/2})_{J=1} \rightarrow (2s^22p^22p_{3/2}^23s_{1/2})_{J=2}$	100.0 <sup>a</sup>
Th <sup>80+</sup>	Ne	$(2s_{1/2}2p^22p^43s_{1/2})_{J=0} \rightarrow (2s^22p^22p_{3/2}^23s_{1/2})_{J=1}$	91.0 <sup>b</sup>
Th <sup>80+</sup>		$(2s_{1/2}2p^22p^43s_{1/2})_{J=1} \rightarrow (2s^22p^22p_{3/2}^23s_{1/2})_{J=1}$	20.0 <sup>a</sup>
Th <sup>80+</sup>		$(2s_{1/2}2p^22p^43d_{3/2})_{J=2} \rightarrow (2s^22p^22p_{3/2}^23d_{3/2})_{J=3}$	19.0
Th <sup>80+</sup>		$(2s_{1/2}2p^22p^43d_{5/2})_{J=2} \rightarrow (2s^22p^22p_{3/2}^23d_{5/2})_{J=2}$	17.0
Th <sup>80+</sup>		$(2s_{1/2}2p^22p^43d_{5/2})_{J=2} \rightarrow (2s^22p^22p_{3/2}^23d_{5/2})_{J=3}$	14.0
Th <sup>80+</sup>		$(2s_{1/2}2p^22p^43d_{5/2})_{J=2} \rightarrow (2s^22p^22p_{3/2}^23d_{5/2})_{J=1}$	13.0

<sup>a</sup>All of the intensity results from the ionization of the  $2s_{1/2}$  electron in sodiumlike ions.

<sup>b</sup>Almost half of the intensity results from the ionization of the  $2s_{1/2}$  electron in sodiumlike ions.

[27]. The device uses an intense electron beam to electrostatically trap, ionize, and excite the thorium. For the present measurements the beam energy was set to 100 keV. This value is well above the 31.3-keV ionization potential of lithiumlike thorium and below the 123.1-keV ionization potential of heliumlike thorium. The beam current was 165 mA. A 3-T magnetic field was employed to squeeze the beam to a 25–30- $\mu\text{m}$  radius, so that the electron density was about  $3 \times 10^{12} \text{ cm}^{-3}$ .

Thorium was introduced into the trap using a metal-vapor arc source [35]. Thorium from this source is ionized no more than a few times. The time required to produce a significant amount of lithiumlike thorium in the interaction with the electron beam can be estimated by solving a set of coupled rate equations for the various charge states of thorium. These rate equations balance ionization and radiative recombination, employing scaling formulas by Lotz and by Kim and Pratt [36,37]. Results of such a calculation are shown in Fig. 1. The estimated time for producing an appreciable amount

of lithiumlike ions is about 5 s, while neonlike ions are produced only in the first second following injection into the trap.

Contributions from charge exchange between neutral background gases in the trap and the thorium ions were not included in the above calculations because the actual amount was not known. Both the speed at which equilibrium is reached and the maximum charge states achievable therefore represent the most favorable circumstances for the production of highly charged thorium ions. Inclusion of charge-exchange recombination into the calculations considerably lengthens the time required to produce the highest charge states and reduces the maximum charge state achievable. As shown below, we have used this dependence on the neutral density to vary the charge-state distribution in the trap. This was necessary in order to generate observable line emission from the lower charge states such as oxygenlike, fluorinelike, and neonlike thorium. We have done so by controlling the pressure in a ballistic gas injector, which produces a colli-

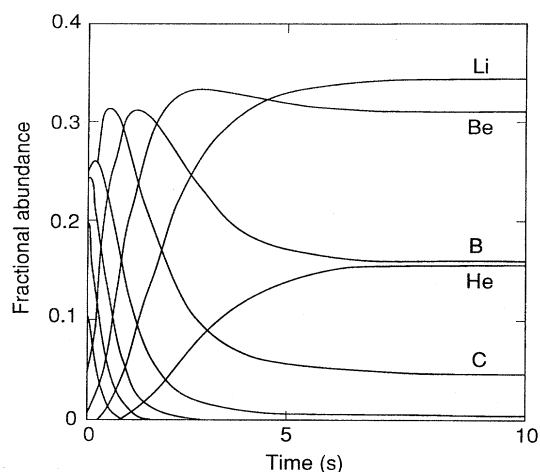


FIG. 1. Calculated evolution of the abundances of highly charged thorium ions. Only ionization and radiative recombination are included in the calculations. The speed of ion production and the maximum ionization states achieved represent, therefore, upper-bound estimates for the production of highly charged thorium ions. The electron energy is 100 keV; the electron current is set at 165 mA.

mated beam of neutral argon atoms that crossed at  $90^\circ$  with the electron beam.

Using the time evolution shown in Fig. 1 as a guide, we started monitoring the x-ray emission 0.2 s after injection, since we are also interested in the x-ray emission from charge states lower than lithiumlike  $\text{Th}^{87+}$ . The thorium was kept in the trap for 30 s. Then the trap was purged and refilled with new thorium from the metal-vapor arc source. Such frequent purging of thorium from the trap was undertaken to prevent buildup of appreciable amounts of barium or tungsten in the trap, which emanate from the electron gun filament.

#### IV. X-RAY EMISSION OF HIGHLY CHARGED THORIUM

The x-ray emission from the ions was monitored via ports that provided direct line-of-sight access to the trap. The ports are located in the plane perpendicular to the beam direction, as shown in Fig. 2. The x-ray instrumentation included a high-purity 50.7-mm diameter, 18.9-mm deep Ge detector, which was used to provide a survey of the x-ray emission. It also included a high-resolution von Hámos-type crystal spectrometer [38], which was used to analyze the thorium  $2p_{3/2} \rightarrow 2s_{1/2}$  emission in detail. The spectrometer employed a  $120 \times 50 \times 0.25 \text{ mm}^3$  LiF(200) crystal with a lattice spacing  $2d = 4.027 \text{ \AA}$ . The crystal was bent to a 30-cm radius of curvature. The diffracted x rays were recorded with a gas-filled proportional counter with a  $10 \times 3 \times 0.4 \text{ cm}^3$  active volume. The working gas consisted of 70% xenon and 30% methane at 1.2-atm overpressure. The resolving power of the setup was about  $\lambda/\Delta\lambda = 2200$ , resulting in line widths of about 1.8–1.9 eV. The resolving power was mainly limited by the 270- $\mu\text{m}$  spatial resolving power of the detector [38]. Line broadening by the thermal ion motion is small and considered negligible in this experiment [39].

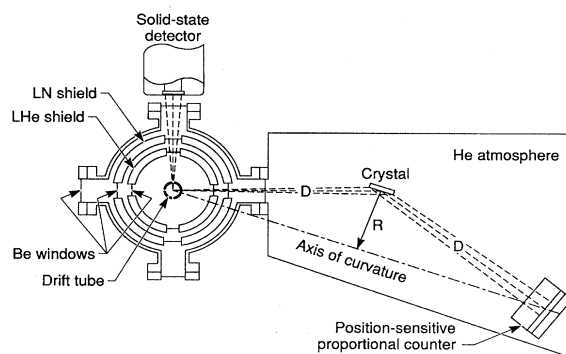


FIG. 2. Schematic layout of the von Hámos-type crystal spectrometer on SuperEBIT. X rays incident upon the crystal are dispersed on the face of the position-sensitive detector. The detector is oriented perpendicular to the line connecting the center of the crystal with the center of the detector to avoid parallax. A high-purity Ge detector concurrently monitors the x-ray emission on a neighboring port. The electron beam propagates in the vertical direction (out of the page) through the center of the drift tube.

#### A. Solid-state detector measurements

The production of very high charge states of thorium was indicated by the observation of photons emitted in the radiative capture of beam electrons into vacancies in the  $L$  shell. Unlike in plasmas with a Maxwellian electron distribution where radiative-recombination photons form a continuum, radiative-recombination photons form distinct lines in EBIT as a result of the monoenergetic electron beam. Moreover, the energy of the radiative recombination x rays lies well above that of characteristic and bremsstrahlung x rays. The radiative-recombination signal thus provides a reliable means for assessing the ionization balance [40].

Two Ge-detector spectra detailing the radiative-recombination lines are shown in Fig. 3. Unlike the spectra recorded in beam-foil measurements, where ions move at relativistic speeds, the SuperEBIT spectra record the actual x-ray energy emitted by the ions, and no Doppler-shift corrections are necessary. Features produced by the radiative capture of beam electrons into the  $n=2$ ,  $n=3$ ,  $n=4$ , and  $n=5$  shells are well resolved. Photons produced by capture into yet higher shells are unresolved and form a smooth transition with the bremsstrahlung continuum that ends at 100 keV, the energy of the electron beam. Superimposed on the bremsstrahlung continuum at 91 and 95 keV are two prominent features, respectively due to the  $2s_{1/2}, 2p_{1/2} \rightarrow 1s_{1/2}$  and  $2p_{3/2} \rightarrow 1s_{1/2} K\alpha$  transitions in highly charged thorium.

The recombination peak into the  $n=2$  shell is split by the spin-orbit interaction into two components: capture into  $j = \frac{3}{2}$  levels and capture into  $j = \frac{1}{2}$  levels. All charge states higher than neonlike have a vacancy in the  $2p_{3/2}$  subshell and thus can, in principle, contribute to the  $j = \frac{3}{2}$  recombination feature. By contrast, only charge states higher than carbonlike with a vacancy in the  $2p_{1/2}$  or  $2s_{1/2}$  subshell can capture an electron into a  $j = \frac{1}{2}$  level and thus are able to contribute to the  $j = \frac{1}{2}$  recombination feature. The relative ratio of the  $j = \frac{1}{2}$  to  $j = \frac{3}{2}$  feature, therefore, presents a measure of the charge balance. This is illustrated in Fig. 3, where a charge balance with a low abundance of the highest charge states is shown

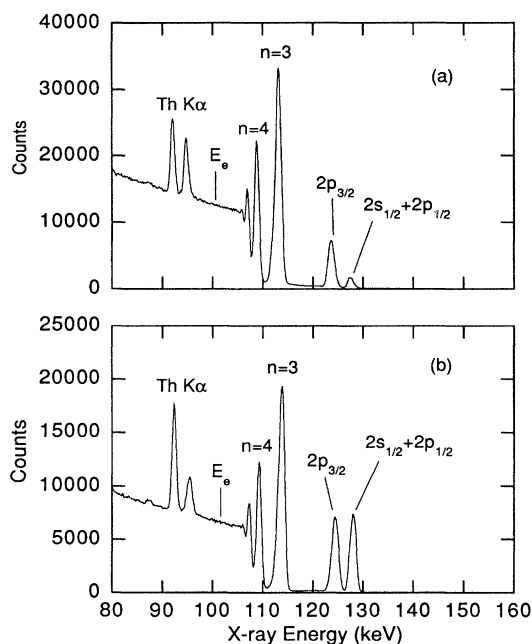


FIG. 3. X-ray emission observed with a high-purity Ge detector. The  $K\alpha$  transitions of highly charged thorium are prominently seen between 90 and 95 keV. The bremsstrahlung background ceases at the energy of the electron beam at 100 keV. Above this energy, features are seen that arise from radiative electron capture. Features from capture into  $n=2, 3, 4$ , and 5 are resolved. Capture into the  $n=2$  shell results in two distinct features separated by nearly 4 keV depending on the angular momentum of the capturing level, i.e.,  $j=\frac{1}{2}$  for capture into  $2s_{1/2}$  and  $2p_{1/2}$  levels and  $j=\frac{3}{2}$  for capture into  $2p_{3/2}$ . The increased intensity of the  $j=\frac{1}{2}$  feature in (b) relative to (a) indicates an ionization balance shifted toward higher charge states, i.e., charge states with vacancies in the  $2p_{1/2}$  and  $2s_{1/2}$  levels. The different ionization balances are the result of different axial trapping potentials and of different gas injector pressures. The beam current is 165 mA for both cases.

in (a) and one with a high abundance is shown in (b). An order-of-magnitude-higher gas-injector pressure and a doubling of the axial trapping potential were used to create the different charge-state abundances.

The Ge-detector spectra allow us to monitor the presence of barium or tungsten in the trap. These two elements emanate continuously from the electron gun filament and are a well known contaminant. At the 100-keV beam energy of the present measurements, the presence of barium is readily ascertained by checking the intensity of the radiative-recombination lines produced in the capture of beam electrons into bare and hydrogenic barium. If present, these lines are located at about 145 keV, i.e., the sum of the ionization energy of the  $1s$  electron in barium and the energy of the beam electrons and thus well isolated from any other feature, as indicated in Fig. 3. Moreover, the presence of barium and tungsten can be ascertained from their respective  $K\alpha$  features situated at 33 and 60 keV. Neither barium (cf. Fig. 3) nor tungsten was detected.

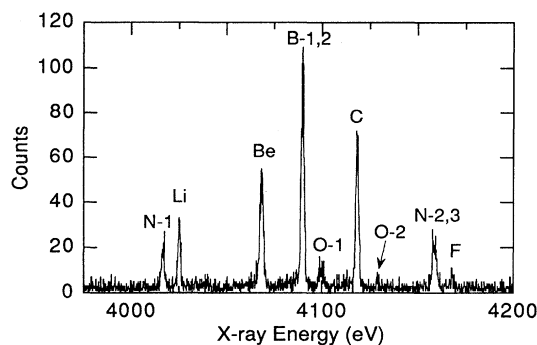


FIG. 4. Crystal-spectrometer spectrum of the  $2s_{1/2}-2p_{3/2}$  transitions in fluorinelike  $\text{Th}^{81+}$  through lithiumlike  $\text{Th}^{87+}$ . The spectrum was obtained for the high-ionization-balance conditions corresponding to Fig. 3(b). The lines are labeled by the ionization stage using the notation of Table I.

### B. Crystal-spectrometer measurements

The total energy range covered collectively by our measurements extended from about 3850 to 4250 eV. A total of eleven distinct features were identified in these spectra formed by the thirteen strongest  $2s_{1/2}-2p_{3/2}$  transitions in the eight charge states from  $\text{Th}^{80+}$  through  $\text{Th}^{87+}$ . In order to observe transitions from all of these ionization stages, it was necessary to vary the charge balance. In particular, we recorded spectra under four different ionization-balance conditions in the trap that range from the low ionization balance of Fig. 3(a) to a balance better than that of Fig. 3(b).

A high-resolution x-ray spectrum of the  $2p_{3/2} \rightarrow 2s_{1/2}$  transitions in thorium is shown in Fig. 4. The notation of Table I is used to label the transitions. The strongest line in the spectrum is from boronlike thorium. Lines from lithiumlike, berylliumlike, and carbonlike thorium are strong as well, while transitions from oxygenlike and fluorinelike thorium are nearly absent. The spectrum corresponds to the case of “high” abundance of high charge states shown in Fig. 3(a).

A high-resolution x-ray spectrum of the  $2p_{3/2} \rightarrow 2s_{1/2}$  transitions corresponding to the case of “low” abundance of high charge states of Fig. 3(b) is shown in Fig. 5. Here, the carbonlike line is the strongest line, followed by nitrogenlike and oxygenlike lines. In addition, weak, unidentified features are seen. Some of these features may be due to transitions in neonlike thorium. However, because of their weak intensity and an uncertainty of about 8 eV in the calculated energies of the neonlike transitions (cf. Sec. VI), they have not been identified. The features may also signify the presence of thorium ions in charge states lower than neonlike in the trap. These features are weaker still or absent in the spectra recorded with a higher abundance of high charge states and do not match the positions of any of the lines from the higher charge states.

The analysis of the uranium  $2s_{1/2}-2p_{3/2}$  spectrum [25] has shown that two features consisted of blends. Each of these blends involved two transitions from the same charge state. The first was a blend of the boronlike lines labeled B-1 and B-2 in Table I; the second was a blend of the nitrogenlike lines labeled N-2 and N-3. The same blends are observed in the thorium spectra. Evidently, varying the charge balance

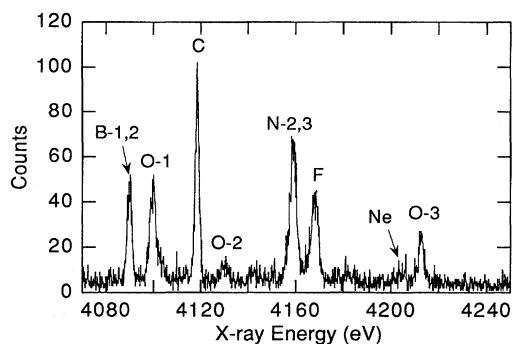


FIG. 5. Crystal-spectrometer spectrum of the  $2s_{1/2}-2p_{3/2}$  transitions in neonlike  $\text{Th}^{80+}$  through boronlike  $\text{Th}^{85+}$ . The spectrum was obtained for the low-ionization-balance conditions corresponding to Fig. 3(a). The lines are labeled by the ionization stage using the notation of Table I. Several weak features are seen that arise from charge states lower than neonlike  $\text{Th}^{80+}$  and are unidentified.

does not provide any help in resolving such blends. While it is impossible to resolve the blend of lines in the boronlike feature, a least-squares fit of two Gaussian-shaped lines was able to resolve the two components of the nitrogenlike feature. The measured ratio of the intensity of N-3 to that of N-2 was 10:3, as predicted in Table I.

In our analysis, we were not able to discern transitions produced by excitation from the berylliumlike metastable level ( $1s^2 2s_{1/2} 2p_{1/2}$ ) $_{J=0}$ . The strongest transitions are predicted to be situated between the lithiumlike and berylliumlike transitions, i.e., near 4061 and 4032 eV. The lines would thus fall in a region free of any other lines, allowing easy identification. However, no corresponding features could be identified. As shown in Table I, our model calculations predict the intensities of such transitions to be weak. Our observations, therefore, are in agreement with these predictions.

## V. CALIBRATION AND EXPERIMENTAL UNCERTAINTIES

The spectra of the thorium  $2s_{1/2}-2p_{3/2}$  transitions were calibrated using transitions in hydrogenlike argon. Specifically, we recorded spectra of the Ly- $\beta$ , Ly- $\gamma$ , Ly- $\delta$  lines spanning a spectral region from about 3935 to 4250 eV. A spectrum showing the hydrogenlike argon transitions is shown in Fig. 6. The argon spectra were recorded in an alternating fashion with the thorium spectra using the same beam energy and beam current. The cycle time between emptying the trap was shortened, however, to 2.8 s to prevent the buildup of high- $Z$  contaminants in the trap. On average, 1 h was spent recording an argon spectrum. This was followed by the recording of a thorium spectrum for 4 h. The recording times for argon lines were significantly shorter because of the higher intensity of the Lyman lines compared to the thorium  $2s_{1/2}-2p_{3/2}$  transitions.

Alternating the spectral measurements between thorium and argon allowed us to test for and assure the stability and reproducibility of the EBIT source, the spectrometer, and the electronics and data acquisition system. We recorded over 30 separate spectra of thorium and as many spectra of argon. Three different spectrometer setups were used in the mea-

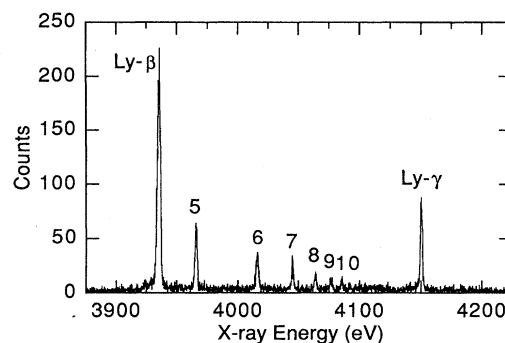


FIG. 6. Crystal-spectrometer spectrum of the Ly- $\beta$  and Ly- $\gamma$  transitions in hydrogenic  $\text{Ar}^{17+}$  used for calibration. Transitions of the type  $1s^2-1snp$  in heliumlike  $\text{Ar}^{17+}$  situated between the  $\text{Ar}^{17+}$  lines are identified by the principal quantum number  $n$  of their upper level.

surement to use different parts of the crystal and the detector to measure the lines. A plot of the position of the  $2s-2p$  transition in boronlike  $\text{Th}^{85+}$  and of Ly- $\beta$  and Ly- $\gamma$  in hydrogenlike argon as a function of run number is given in Fig. 7. Error bars indicate statistical uncertainties only. As the figure illustrates, the measured line positions were reproducible typically within about a tenth of an electron volt. Drifts in the spectrometer and the response of the electronics were not noted.

The lines of hydrogenlike argon represent a good choice for calibration because their energies are theoretically well known. Hydrogenic systems are the simplest atomic systems, and both the Dirac and QED energies can be calculated with

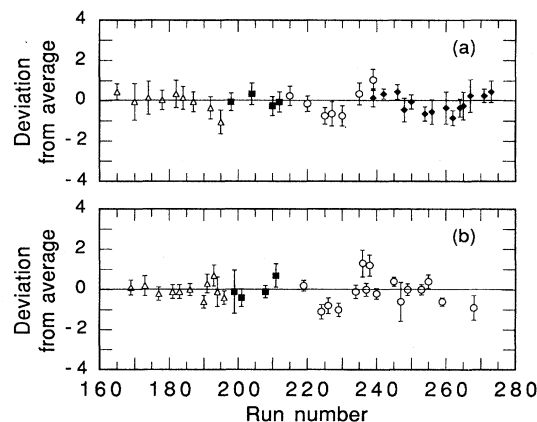


FIG. 7. Stability of the measured line position throughout the measurement period. (a) Lines of hydrogenlike argon: the Ly- $\beta$  line is represented by open triangles, solid squares, and open circles and the Ly- $\gamma$  line is represented by solid diamonds. The detector was moved after runs 196, 212, and 220, as indicated by different symbols. The analyzing crystal was turned after run 236, eliminating the argon Ly- $\beta$  line from the analyzed spectral region. (b) Line B of boronlike thorium. Plotted are the differences from the average line positions (in pixel number, where one pixel equals about 0.31 eV). Uncertainty limits are statistical only.

the highest precision. The energy of the  $1s$  ground state of hydrogenlike argon has been calculated, for example, by Garcia and Mack [41], Erickson [42], and Johnson and Soff [43]. These values differ by no more than 0.0143 eV, and the differences arise, for the most part, from readjustments of the fundamental physical constants, such as the Rydberg constant, over the past 30 years. The total QED contribution to the  $1s$  ground state is a mere 1.14 eV. A measurement of this contribution was made by Briand *et al.* [44] with an accuracy of 0.5 eV and later by Beyer *et al.* [45] and Marmar *et al.* [46] with an accuracy of 0.02 and 0.04 eV, respectively. In each case, agreement with the calculated value was found.

For the calibration of the thorium spectra, we are interested in the transition energies of the Ly- $\beta$ , Ly- $\gamma$ , and Ly- $\delta$  lines (cf. Fig. 6). We used 3935.72, 4150.33, and 4249.69 eV for the  $P_{3/2}$  component and 3934.30, 4149.74, and 4249.38 eV for the  $P_{1/2}$  component, respectively, of each line. These transition energies are based on the calculations by Erickson [42] and have been adjusted for the most recent changes in the values of the physical constants. To convert between wavelength and energy, we used the conversion constant [47]  $hc = 12\,398.42$  eV Å.

Because the resolving power of the spectrometer was insufficient to clearly resolve the  $P_{3/2}$  and  $P_{1/2}$  components, it was necessary to use an intensity-weighted average transition energy for each Lyman line. The ratio of the excitation cross sections of  $P_{3/2}$  and  $P_{1/2}$  components is 2:1. The actual intensity ratio of the two components observed on EBIT, however, differs from this ratio for two reasons. First, the x-ray emission is generally nonisotropic. Second, it is polarized. The two effects are interrelated and a result of the directionality introduced to electron-ion interactions by the electron beam [48–50]. The sensitivity to the effects of polarization was enhanced in the present measurement because the lines were recorded at a Bragg angle close to  $45^\circ$ , i.e., close to the angle at which one of the two electric-field components is being extinguished in the crystal.

In the case of the Ly- $\beta$  lines, it was possible to discern the Ly- $\beta_1$  and Ly- $\beta_2$  components with the help of a least-squares-fitting routine. The ratio of the intensities of the two components was found to be  $1.69 \pm 0.10$ , i.e., about 15% lower than the ratio of 2.00 expected from their respective excitation cross sections.

The measured ratio of the Ly- $\beta_1$  and Ly- $\beta_2$  components is validated by our calculations of the magnetic sublevel populations using the code developed by Zhang, Sampson, and Clark [51]. The results of these calculations are listed in Table II. From these results we can compute the polarization  $P$  of the  $J=3/2$  components using the equation

$$P_{3/2} = \frac{3(\sigma_{1/2} - \sigma_{3/2})}{3\sigma_{3/2} + 5\sigma_{1/2}}, \quad (1)$$

where  $\sigma_{1/2}$  and  $\sigma_{3/2}$  are the cross sections for excitation of the magnetic sublevels  $m_J = \frac{1}{2}$  and  $m_J = \frac{3}{2}$ , respectively. We find about  $P_{3/2} = -6.5\%$  in each case. By contrast, the  $J = \frac{1}{2}$  component is unpolarized. The fact that the  $J = \frac{3}{2}$  component is negatively polarized at electron energies of 100 keV (25 times threshold) contrasts starkly with the positive values determined for its polarization near the excitation threshold, where  $P_{3/2} \approx +65\%$  [52]. The negative value is, however,

TABLE II. Fully relativistic cross sections for  $1s$ - $np$  excitation of the magnetic sublevel in hydrogenlike argon at electron energies of 100 keV. Values are given for  $n=3, 4$ , and 5 in units of  $\text{cm}^2$ . Cross sections for states with negative values of  $m_J$  equal those for states with positive values of  $m_J$  and are not listed.

Configuration \ $m_J$	1/2	3/2
$3p_{1/2}$	$9.43 \times 10^{-24}$	
$3p_{3/2}$	$8.71 \times 10^{-24}$	$10.31 \times 10^{-24}$
$4p_{1/2}$	$3.34 \times 10^{-24}$	
$4p_{3/2}$	$3.08 \times 10^{-24}$	$3.67 \times 10^{-24}$
$5p_{1/2}$	$1.58 \times 10^{-24}$	
$5p_{3/2}$	$1.45 \times 10^{-24}$	$1.75 \times 10^{-24}$

consistent with the dropoff noted for electron energies well above threshold [52]. From the values of the polarization of each component we can compute the ratio  $I_{3/2}^{\text{obs}}/I_{1/2}^{\text{obs}}$  of the observed intensities by following the formalism described in Ref. [53]. In particular,

$$\frac{I_{3/2}^{\text{obs}}}{I_{1/2}^{\text{obs}}} = \frac{(1 + P_{3/2}) + R(1 - P_{3/2})}{(1 + P_{1/2}) + R(1 + P_{1/2})} \frac{3 - P_{1/2} \langle I_{3/2} \rangle}{3 - P_{3/2} \langle I_{1/2} \rangle}. \quad (2)$$

Here,  $R$  is the ratio of the integrated crystal reflectivities for x rays polarized parallel and perpendicular to the plane of dispersion ( $R \approx 0$  for our measurement near  $45^\circ$ ), and  $\langle I_{3/2} \rangle / \langle I_{1/2} \rangle$  is the  $4\pi$ -averaged ratio of the components, i.e.,  $\langle I_{3/2} \rangle / \langle I_{1/2} \rangle = 2$ . The calculated values of  $I_{3/2}^{\text{obs}}/I_{1/2}^{\text{obs}}$  are 1.83. This value is slightly higher than the measured ratio of  $1.69 \pm 0.10$  for the Ly- $\beta$  components. This is not surprising, as the calculation takes into account only impact excitation. At an electron energy of 100 keV we expect a large population of bare argon in the trap. Radiative electron capture into levels with high quantum numbers disproportionately enhances the  $J = \frac{1}{2}$  component [54] and thus may further lower the actual ratio.

Using the measured ratio for the intensities of the  $P_{3/2}$  and  $P_{1/2}$  components, we obtained 3935.19, 4150.11, and 4249.57 eV for the intensity-weighted energies of the Ly- $\beta$ , Ly- $\gamma$ , and Ly- $\delta$  lines, respectively. In the following these values were employed in the calibration of the thorium spectra. For comparison, the intensity-weighted energies based on the “standard” ratio of 2:1 are 0.05, 0.03, and 0.01 eV, respectively, higher than the actual values for calibration. In estimating the accuracy of the reference energies, we conservatively assumed an uncertainty of 0.06 eV, i.e., a value that is *twice* the average difference between the two ways of calculating the intensity-averaged energies.

#### A. Experimental thorium energies

Using the hydrogenic argon lines for calibration, we obtained the values listed in Table III for the thorium  $2s$ - $2p$  transitions. Having ascertained the absence of systematic drifts in the electronics or spectrometer, the uncertainty in the measured energies of the thorium  $2s$ - $2p$  transitions is given by the quadrature sum of four contributions: the statistical uncertainties of the positions of the thorium lines, the statistical uncertainties of the positions of the calibration lines, the systematic uncertainties associated with the uncer-

TABLE III. Summary of measured energies of the  $2s_{1/2}-2p_{3/2}$  transitions in Th<sup>80+</sup> through Th<sup>87+</sup> (in eV). Theoretical values are from multiconfiguration Dirac-Fock calculations. The given uncertainties represent 68% confidence limits. The contributions arising from the counting statistics included in the limits are listed separately inside parentheses.

Key	Ion	Upper level	$E_{\text{expt}}$	$E_{\text{theory}}$	$E_{\text{theory}}-E_{\text{expt}}$
Li	Th <sup>87+</sup>	$(2p_{3/2})_{J=3/2}$	$4025.23 \pm 0.14 (\pm 0.06)$	4027.0	+1.8
Be	Th <sup>86+</sup>	$(2s_{1/2}2p_{3/2})_{J=1}$	$4068.47 \pm 0.13 (\pm 0.03)$	4071.7	+3.2
B-1	Th <sup>85+</sup>	$(2s_{1/2}2p_{1/2}2p_{3/2})_{J=3/2}$	$4089.92 \pm 0.50^a$	4093.3	+3.4
B-2	Th <sup>85+</sup>	$(2s_{1/2}2p_{1/2}2p_{3/2})_{J=1/2}$	$4089.92 \pm 0.50^a$	4092.9	+3.0
B-1,2	Th <sup>85+</sup>	blend	$4089.92 \pm 0.13 (\pm 0.02)$	4093.2	
C	Th <sup>84+</sup>	$(2s_{1/2}2p_{1/2}^2 2p_{3/2})_{J=1}$	$4118.43 \pm 0.13 (\pm 0.02)$	4122.1	+3.7
N-1	Th <sup>83+</sup>	$(2s_{1/2}2p_{1/2}^2 2p_{3/2}^2)_{J=5/2}$	$4016.67 \pm 0.13 (\pm 0.04)$	4019.0	+2.3
N-2	Th <sup>83+</sup>	$(2s_{1/2}2p_{1/2}^2 2p_{3/2}^2)_{J=1/2}$	$4157.20 \pm 0.26 (\pm 0.10)$	4161.5	+4.3
N-3	Th <sup>83+</sup>	$(2s_{1/2}2p_{1/2}^2 2p_{3/2}^2)_{J=3/2}$	$4159.49 \pm 0.21 (\pm 0.08)$	4163.4	+3.9
N-2,3	Th <sup>83+</sup>	blend	$4159.00 \pm 0.03 (\pm 0.03)$		
O-1	Th <sup>82+</sup>	$(2s_{1/2}2p_{1/2}^2 2p_{3/2}^3)_{J=2}$	$4099.60 \pm 0.20 (\pm 0.04)$	4103.4	+3.8
O-2	Th <sup>82+</sup>	$(2s_{1/2}2p_{1/2}^2 2p_{3/2}^3)_{J=1}$	$4129.94 \pm 0.15 (\pm 0.08)$	4133.2	+3.3
O-3	Th <sup>82+</sup>	$(2s_{1/2}2p_{1/2}^2 2p_{3/2}^3)_{J=1}$	$4212.80 \pm 0.13 (\pm 0.06)$	4217.4	+4.6
F	Th <sup>81+</sup>	$(2s_{1/2}2p_{1/2}^2 2p_{3/2}^4)_{J=1/2}$	$4168.06 \pm 0.24 (\pm 0.08)$	4172.7	+4.6
Ne	Th <sup>80+</sup>	$(2s_{1/2}2p_{1/2}^2 2p_{3/2}^4 3s_{1/2})_{J=0}$	$4204.92 \pm 0.43 (\pm 0.13)$	4210.4	+5.5

<sup>a</sup>Transition was not resolved. The listed uncertainty corresponds to the maximum value assuming that the blend consists of two lines with a disparity in intensity that does not exceed 3:1.

tainties in the wavelengths of the hydrogenlike calibration lines, and uncertainties arising from nonlinearities in the detector response. An overview of the individual contributions to the uncertainty of the lithiumlike  $2s_{1/2}-2p_{3/2}$  transition is given in Table IV. The overall statistical uncertainty in the measured line positions from all runs is 0.055 eV. The statistical uncertainty in the line positions of the calibration lines adds 0.060 eV. In addition, there is a 0.06-eV contribution from the uncertainty in the absolute energy of the calibration lines, as discussed above. We stress that the magnitude of the latter two contributions is different for different thorium lines and depends on the line's location relative to the calibration lines. Finally, there is a 0.10-eV contribution from the integral nonlinearity in the detector response. The value of this contribution corresponds to the measured spatial linearity of 20  $\mu\text{m}$  for the detector employed in our spectrometer, and represents a conservative estimate, as shown in Ref. [55]. We have also checked for line shifts caused by blending with lines. However, we found no evidence of blending with other lines for the  $2s_{1/2}-2p_{3/2}$  transition in lithiumlike Th<sup>87+</sup>. Adding all contributions in quadrature gives an uncertainty of 0.14 eV for uncertainty of the measured energy of the lithiumlike transition. As given in Table IV, the energy measured for this line is  $4025.23 \pm 0.14$  eV. The accuracy of our measurement thus is 35 ppm. Although some of the assumptions

TABLE IV. Contributions to the 0.14-eV uncertainty in the measured energy of the  $2s_{1/2}-2p_{3/2}$  transitions in lithiumlike Th<sup>87+</sup>.

Source	Magnitude (eV)
Position of thorium line	0.055
Position of calibration lines (dispersion)	0.060
Uncertainty in energies of calibration lines	0.060
Detector linearity	0.100
Blending with other lines	0.000

entering the determination of the individual contributions to the total uncertainties of our measurements were set at conservatively high values, we consider the total uncertainties to represent 68% confidence limits. Estimating the uncertainties in the  $2\text{-}\sigma$  confidence limit, we find  $4025.23 \pm 0.19$  eV.

The uncertainties in the measured energies of the  $2s_{1/2}-2p_{3/2}$  transitions in the charges states of thorium lower than lithiumlike are of comparable magnitude, as shown in Table III. The total error varies from  $\pm 0.13$  to  $\pm 0.50$  eV. For comparison, the statistical uncertainty of the individual line positions varies from as little as 0.02 eV for the strong boronlike and carbonlike thorium lines to as much as 0.13 eV for the two weak neonlike thorium lines. In most cases where the statistical uncertainty is small, the total error is dominated by the estimated 0.1-eV uncertainty in the integral nonlinearity of the proportional counter. In several cases, the uncertainty was dominated by blends with other lines. In particular, blends were a factor in determining the line positions of the oxygenlike line O-1, the fluorinelike line F, and the neonlike line Ne. Here, blends added 0.15, 0.20, and 0.40 eV, respectively, to the uncertainty of the measurements. Blending also increased the uncertainty of the inferred wavelengths of the nitrogenlike lines N-2 and N-3.

## B. Test with heliumlike argon

A check of the accuracy of our measurement technique is provided by a measurement of the energies of the high- $n$  transitions of heliumlike argon. The series of the heliumlike transitions  $1snp \ ^1P_1 \rightarrow 1s^2 \ ^1S_0$  for  $n \geq 5$  is clearly seen in the argon spectrum in Fig. 6. We determined the energies of the six transitions with  $n=5-10$ , which were well resolved by the spectrometer. The results are listed in Table V.

Our measured values of the energies of the high- $n$  transitions of heliumlike argon can be compared to the results from earlier measurements of Seely and Feldman [56], which

TABLE V. Comparison of measured and predicted energies of the  $1s^2\ 1S_0-1snp\ 1P_1$  transitions in heliumlike  $\text{Ar}^{16+}$  for  $n=5-10$ . All values are in eV. The given uncertainties represent 68% confidence limits. The contributions arising from the counting statistics included in the limits are listed separately inside parentheses.

$n$	Present	$E_{\text{expt}}$	$E_{\text{theory}}$
		Seely and Feldman Ref. [56]	
5	$3963.21 \pm 0.14$ ( $\pm 0.04$ )	$3963.09 \pm 0.25$	3963.327
6	$4011.33 \pm 0.14$ ( $\pm 0.05$ )	$4011.25 \pm 0.26$	4011.399
7	$4040.25 \pm 0.15$ ( $\pm 0.07$ )	$4040.28 \pm 0.26$	4040.387
8	$4059.19 \pm 0.16$ ( $\pm 0.09$ )	$4059.16 \pm 0.42$	4059.202
9	$4072.16 \pm 0.18$ ( $\pm 0.13$ )	$4071.65 \pm 0.51$	4072.102
10	$4081.44 \pm 0.19$ ( $\pm 0.14$ )	$4081.77 \pm 0.46$	4081.328

are listed in Table V. Their results were obtained from solar flare spectra and have uncertainties that are about twice those of our measurements. Very good agreement with their values can be noted.

Our measurements can also be compared to theoretical values. The transition energies of the heliumlike ions are not as well known as those of the hydrogenlike ions. The theoretical energies listed in Table V were obtained with the help of a semiempirical scaling formula described and tested by Martin [57]. The accuracy of the heliumlike transition energies estimated with this formula is likely to be better than 0.05 eV. In the high- $n$  limit, this formula converges to the  $1s^2$  ground-state energy. For this we used a value of 4120.659 eV, as calculated by Drake [58]. This value is virtually identical to a more recent calculation by Plante, Johnson, and Sapirstein [59]. It is, however, 0.07 eV less than the recent calculation of Cheng *et al.* [60], and the formula would predict accordingly higher energies, if we had used their value for the  $1s^2$  ground-state energy.

The differences between measured and calculated energies of the  $1snp\ 1P_1 \rightarrow 1s^2\ 1S_0$  transitions in heliumlike argon are shown in Fig. 8. Agreement between measured and calculated transition energies is excellent. The largest difference is 0.14 eV. Although this difference falls outside of the limits given by the statistical uncertainty in the measured line position, it falls well within the combined statistical and systematic uncertainty limits, which are listed for each transition in Table V. As for the thorium lines, the combined statistical and systematic uncertainty limits represent the quadrature sum of the statistical uncertainties of the heliumlike line positions, the statistical uncertainties of the line positions of the calibration lines, the systematic uncertainties arising from the uncertainties associated with the wavelengths of the hydrogenlike calibration lines, and uncertainties arising from nonlinearities in the detector response. The magnitude of the latter three uncertainties are about 0.06, 0.06, and 0.10 eV, respectively, as discussed above for the  $2s-2p$  transition in lithiumlike  $\text{Th}^{87+}$ .

The lithiumlike  $\text{Th}^{87+}$  transition is situated between the  $n=6$  and  $n=7$  transitions. The uncertainty limits ( $\pm 0.14$  eV) assigned to it are larger than any of the differences between measured and calculated energies for the heliumlike argon transitions. The agreement between measured and calculated energies for the heliumlike argon transitions represents

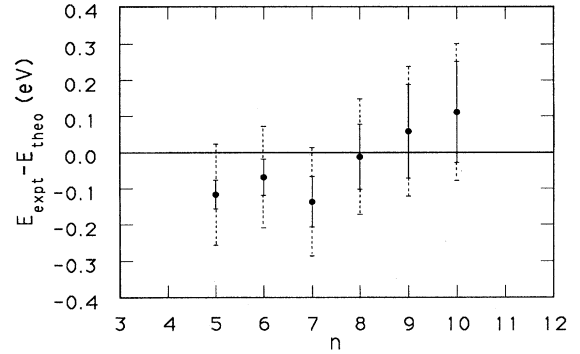


FIG. 8. Difference between measured and predicted energies of the  $1s^2-1snp$  ( $5 \leq n \leq 10$ ) transitions in heliumlike  $\text{Ar}^{16+}$ . Uncertainties from counting statistics are indicated by solid vertical lines, combined statistical and systematic uncertainties by dashed vertical lines. The uncertainty in the theoretical transition energies, estimated at about 0.1 eV, is not shown. The position of the  $2s_{1/2}-2p_{3/2}$  transition in lithiumlike  $\text{Th}^{87+}$  falls in between the  $n=6$  and  $n=7$   $\text{Ar}^{16+}$  lines.

sents an independent test and a validation of the accuracy we achieved in determining the wavelengths of the thorium  $2s-2p$  transitions and may indicate that our uncertainty estimate exceeds the 68% confidence limit.

Another way to assess the accuracy of the measured energy of the lithiumlike  $\text{Th}^{87+}$  transition is to use the heliumlike transitions for calibration. Employing the theoretical values listed in Table V as reference values, we get  $4025.29 \pm 0.19$  eV. Had we used the value of the  $1s^2$  ground-state energy calculated by Cheng *et al.* [60] in computing the heliumlike transition energies, we would have gotten  $4025.36 \pm 0.19$  eV. Either value is in good agreement within uncertainty limits with the value of  $4025.23 \pm 0.14$  eV determined relative to the hydrogenic reference lines. We note that the uncertainties are higher in the case of the heliumlike reference lines because of the added uncertainty in the scaling formula and the  $1s^2$  ground-state energy.

## VI. COMPARISON WITH THEORY

A systematic calculation of the screened self-energy and vacuum polarization for lithiumlike ions was reported recently by Blundell [13]. For the  $2s_{1/2}-2p_{3/2}$  transitions in lithiumlike  $\text{Th}^{87+}$ , Blundell calculated  $-35.87$  eV for the total QED energy, which included  $-49.26$  eV from the self-energy term. This was added to the non-QED energy of 4060.98 eV to yield 4025.10 eV with an uncertainty of 0.04 eV estimated from higher-order contributions missing in the QED calculations [13]. This value is in excellent agreement with our measured value of  $4025.23 \pm 0.14$  eV. By contrast, a value of 4024.96 eV was calculated by Kim *et al.* [61], which included  $-36.02$  eV for the total QED energy. These authors used Dirac-Fock energies corrected by relativistic correlation and approximate QED energies based on scaled hydrogenic values [61]. Their value differs from Blundell's value by merely 0.14 eV. However, it disagrees with our measured value by  $0.27 \pm 0.14$  eV. Because of the high precision achieved in our measurement, we are thus able to

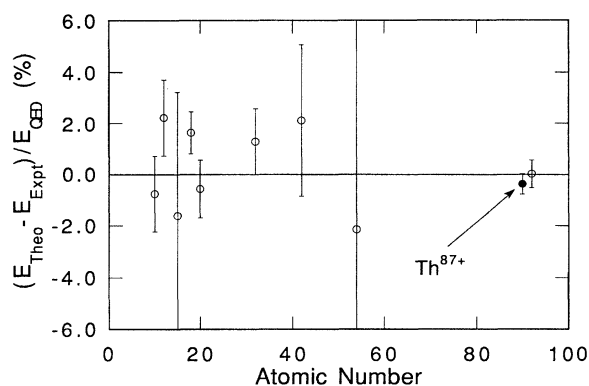


FIG. 9. Difference between measured and predicted energies of the  $2s_{1/2}-2p_{3/2}$  transitions in lithiumlike ions expressed as a fraction of the QED contribution. Theoretical energies are from Blundell and co-workers (Ref. [13,17]). Experimental values for  $Z \leq 54$  are from Edlén [63], Hinnov *et al.* [64], and Martin *et al.* [29]. The uncertainty limits of the uranium value reflect the 68% confidence limit given in Ref. [26]. The present result is displayed as a solid circle.

distinguish between the two theoretical values. Such a distinction was not possible in our earlier measurement of lithiumlike  $U^{89+}$  [25]. We can also compare our measurement to the value calculated by Indelicato and Desclaux [62] using methods similar to Kim *et al.* Their value of 4026.26 eV is 1.03 eV larger than our measured value and thus differs markedly.

A comparison between the values calculated by Blundell [13] and previous measurements of the energies of the  $2s_{1/2}-2p_{3/2}$  transitions in various elements is given in Fig. 9. The previous measurements include values reported by Edlén [63], Hinnov *et al.* [64], and Martin *et al.* [29], and extend up to xenon ( $Z=54$ ). Also included in the figure is our recent measurement of the  $2s_{1/2}-2p_{3/2}$  transition in lithiumlike  $U^{89+}$  [25,26], which is compared to a value calculated by Blundell, Johnson, and Sapirstein [17]. In the figure, we plotted the difference between calculated transition energies and measurement expressed as a fraction of the size of the calculated QED contribution for each transition. The figure shows that our present measurement of  $Th^{87+}$  represents the most sensitive test of the calculated QED contributions for the  $2s_{1/2}-2p_{3/2}$  transition to date. In particular, given a calculated value of  $-35.87$  eV for the total QED contributions, our present measurement represents a 0.39% test.

The agreement between the measured values and values calculated by Blundell for the  $2s_{1/2}-2p_{3/2}$  transitions in  $Th^{87+}$  and  $U^{89+}$  is significant because such a close agreement is not found between the measured and calculated values for the  $2s_{1/2}-2p_{1/2}$  transition in lithiumlike  $U^{89+}$ . Here Scheppe *et al.* measured  $280.59 \pm 0.10$  eV [21], which differs by 0.24 eV from the value of  $280.83 \pm 0.10$  calculated by Blundell [13]. We note that the effects of core relaxation, nuclear recoil, and nuclear polarization affect the value of the calculated QED contribution by about 0.1–0.3 eV. For example, the effect of nuclear polarization in uranium was calculated to shift the  $2s_{1/2}-2p_{1/2}$  splitting by about 0.18 eV [65], while nuclear recoil in uranium contributes  $-0.08$  eV

[11]. A precise calculation of these effects for thorium has not been made, to our knowledge. These contributions could easily nullify the agreement between measurement and calculations. Moreover, a recent large-scale relativistic configuration interaction (CI) calculation found differences of up to 0.35 eV for the Breit energies calculated with either the CI or the RMBPT used by Blundell [66]. The same study found a difference of 0.57 eV with the QED energy calculated by Blundell for the  $2s_{1/2}-2p_{3/2}$  transition in  $Th^{87+}$  [66]. This study suggests that inaccuracies in the Coulomb, Breit, and QED energies may be masked because of partial cancellations. A definitive comparison of experimental data with theoretical predictions on the 0.1-eV level thus has yet to be made.

The measurements of the  $2s_{1/2}-2p_{3/2}$  transition energies in berylliumlike  $Th^{86+}$  through neonlike  $Th^{80+}$  provide important information for testing relativistic correlation energies and QED calculations in highly charged ions with more than one valence electron. A standard method of calculating the structure of such open-shell ions is the multiconfiguration Dirac-Fock approach [67]. A comparison of the  $2s_{1/2}-2p_{3/2}$  transition energies calculated using this method with the values measured for berylliumlike  $U^{88+}$  through neonlike  $U^{82+}$  in Ref. [25] showed a significant difference. This difference increased for the lower charge states, and was found to be 8.0 eV for the  $2s_{1/2}-2p_{3/2}$  transition energy of neonlike  $U^{82+}$  [25]. Part of the difference, amounting to about 2 eV, could be attributed to inadequacies of computing the QED energies. The remainder, however, was attributed to residual correlation energies [25].

In order to verify the findings in Ref. [25], we have performed similar calculations for the  $2s_{1/2}-2p_{3/2}$  transition energies in berylliumlike  $Th^{86+}$  through neonlike  $Th^{80+}$ . We computed the energies of the  $2s_{1/2}-2p_{3/2}$  transitions in  $Th^{87+}$  through  $Th^{80+}$  using the MCDF code of Grant and co-workers [68,69]. The calculations were performed in the optimal level (OL) approach by including configurations of the type  $1s^2 2s^m 2p^n$ ; in the case of  $Th^{80+}$ , also configurations of the type  $1s^2 2s^2 2p^6 3l$  and  $1s^2 2s^2 2p^5 3l$  were included. The QED corrections were calculated in the extended-average level scheme [68]. This was necessary because in the OL approach a small difference in the effective

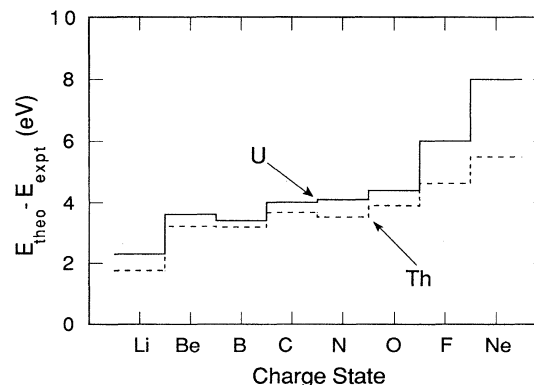


FIG. 10. Average difference between measured  $2s_{1/2}-2p_{3/2}$  transition energies and values predicted with the MCDF method for the lithiumlike through neonlike charge states of thorium and uranium.

charge seen by the  $1s$  electron in the initial and final states resulted in an unphysically large change in the self-energy correction. Nuclear finite size corrections were taken into account by using a Fermi charge distribution with parameters given by Johnson and Soff [43]; finite nuclear size corrections to the self-energy were included by using the values from Mohr and Soff [5]. The resulting transition energies are listed in Table III. Here, we also list the discrepancies between theoretical and measured values. Like for the measurements of uranium [25], significant discrepancies are found, which increase for the lower charge states.

To illustrate the differences between the MCDF calculations and measurements, the average differences are displayed for each charge state in Fig. 10. Here we also show the average differences found for uranium in Ref. [25]. The thorium results track those of uranium, affirming the conclusions drawn in Ref. [25]. The average differences for thorium, however, are consistently lower than those for uranium. The smallest error in computing relativistic correlation energies is made in calculating the  $2s_{1/2}-2p_{3/2}$  transition in lithiumlike  $\text{Th}^{87+}$ . Comparing the MCDF value for this transition to the measured value, we can estimate the error in the value for the QED energy calculated by the MCDF method. The difference between the calculated and measured transition energies is  $E_{\text{theory}} - E_{\text{expt}} = 1.8$  eV. As shown by Kim *et al.* [61], the electron correlation energy for this transition is no more than 0.2 eV. Thus, we estimate that the QED contribution calculated by the MCDF approach is underestimated by about 1.6 eV. This value is 0.5 eV lower than that estimated for uranium, resulting in a consistently lower average difference with theory than that noted for uranium.

While the MCDF approach has been the method of choice for most open-shell ions, more accurate methods for calculating the atomic structures of highly charged ions have been implemented recently by Johnson, Sapirstein, and Cheng [19]. These authors have applied the MBPT approach to calculating the Dirac energies of the  $2s_{1/2}-2p_{3/2}$  transitions in berylliumlike, carbonlike, fluorinelike, and neonlike uranium ions. Unlike MCDF energies, their approach provided good agreement with measurements with differences ranging from 0.1 to 0.6 eV [19]. An exception was the calculated value for berylliumlike  $\text{U}^{88+}$ , for which the MBPT approach converged poorly. For this case, a large-scale relativistic CI calculation was carried out by Chen *et al.*, which differed from the experiment by only 0.1 eV [70]. No such calculations have yet, to our knowledge, been reported for the analogous  $2s_{1/2}-2p_{3/2}$  transitions in thorium. The present thorium measurements thus serve as a second set of benchmarks for testing these calculational approaches. Together with our earlier uranium measurements, the present measurements can serve to guide the development of precise theoretical methods for calculating the structure of highly charged ions.

## VII. CONCLUSION

We have presented high-resolution crystal spectrometer measurements of thirteen transitions in eight ionization stages  $\text{Th}^{80+}$  through  $\text{Th}^{87+}$ . The data confirm line identifications and transition energy measurements made in an earlier study of uranium [25] and provide a second independent benchmark for testing theoretical approaches for calculating the structure of highly charged ions.

A detailed analysis of the experimental uncertainties was given. The reliability of the uncertainty limits was tested and validated in a measurement of the  $1s^2-1snp$  ( $n \leq 10$ ) transitions in heliumlike  $\text{Ar}^{16+}$ . The typical accuracy of 35 ppm was achieved in our measurement of the thirteen  $2s_{1/2}-2p_{3/2}$  transition energies. As a result, our measurements represent the most sensitive test of the calculated QED contributions for the  $2s_{1/2}-2p_{3/2}$  transitions to date. In fact, our measurements test the accuracy of the QED calculations in the limit  $(Z\alpha) \approx 1$  with a degree of accuracy that is about sixty times higher than current measurements of the QED contributions to the  $1s$  ground state in hydrogenlike  $\text{U}^{91+}$ . For the case of lithiumlike  $\text{Th}^{87+}$ , where the calculated value for the total QED contributions is about 36 eV, our present measurement represents a 0.39% test. The accuracy of our measurements is comparable to the effects of nuclear polarization, nuclear recoil, and variations in nuclear size. It is thus conceivable to probe and isolate nuclear effects in future measurements.

As mentioned above, to our knowledge, no data exist yet for the  $2s_{1/2}-2p_{3/2}$  transitions in lithiumlike ions with atomic number in the range  $54 < Z < 90$ . Neither are there any measurements in this range of atomic numbers of the  $2s_{1/2}-2p_{3/2}$  transitions in the charge states lower than lithiumlike. For the development of appropriate theoretical methods that provide accurate energy-level estimates for highly charged ions, further, systematic high-precision measurements along the isoelectronic sequence will be needed. As our present measurements have shown, the relative simplicity of the trapped-ion approach allows these much needed studies, both along the isoelectronic as well as along the isonuclear sequence.

## ACKNOWLEDGMENTS

We are grateful for the encouragement and support received from Mark Eckart and Andy Hazi during the course of these measurements. This work was performed under the auspices of the Department of Energy at Lawrence Livermore National Laboratory under Contract No. W-7405-ENG-48 and was in part supported by the Office of Basic Energy Sciences of the U.S. Department of Energy.

- 
- [1] G. W. Erickson, Phys. Rev. Lett. **27**, 780 (1971).  
 [2] P. J. Mohr, Phys. Rev. Lett. **34**, 1050 (1975).  
 [3] P. J. Mohr and Y.-K. Kim, Phys. Rev. A **45**, 2727 (1992).  
 [4] P. J. Mohr, Phys. Rev. A **46**, 4421 (1992).

- [5] P. J. Mohr and G. Soff, Phys. Rev. Lett. **70**, 158 (1993).  
 [6] E. G. Kessler, Jr., R. D. Deslattes, D. Girard, W. Schwitz, L. Jacobs, and O. Renner, Phys. Rev. A **26**, 2696 (1982).  
 [7] E. Lindroth and P. Indelicato, Phys. Scr. **T46**, 139 (1993).

- [8] P. Indelicato and E. Lindroth, *Phys. Rev. A* **46**, 2426 (1992).
- [9] K. T. Cheng, W. R. Johnson, and J. Sapirstein, *Phys. Rev. Lett.* **66**, 2960 (1991).
- [10] D. K. McKenzie and G. W. F. Drake, *Phys. Rev. A* **44**, R6973 (1991).
- [11] S. A. Blundell, *Phys. Rev. A* **46**, 3762 (1992).
- [12] K. T. Cheng, W. R. Johnson, and J. Sapirstein, *Phys. Rev. A* **47**, 1817 (1993).
- [13] S. A. Blundell, *Phys. Rev. A* **47**, 1790 (1993).
- [14] W. R. Johnson, S. A. Blundell, and J. Sapirstein, *Phys. Rev. A* **37**, 2764 (1988).
- [15] W. R. Johnson, S. A. Blundell, and J. Sapirstein, *Phys. Rev. A* **38**, 2699 (1988).
- [16] W. R. Johnson, S. A. Blundell, and J. Sapirstein, *Phys. Rev. A* **4**, 1087 (1990).
- [17] S. A. Blundell, W. R. Johnson, and J. Sapirstein, *Phys. Rev. A* **41**, 1698 (1990).
- [18] M. H. Chen, K. T. Cheng, and W. R. Johnson, *Phys. Rev. A* **47**, 3692 (1993).
- [19] W. R. Johnson, J. Sapirstein, and K. T. Chen, *Phys. Rev. A* **51**, 297 (1995).
- [20] C. T. Munger and H. Gould, *Phys. Rev. Lett.* **57**, 2927 (1986).
- [21] J. Schweppe, A. Belkacem, L. Blumenfeld, N. Claytor, B. Feinberg, H. Gould, V. E. Kostroun, L. Levy, S. Misawa, J. R. Mowat, and M. H. Prior, *Phys. Rev. Lett.* **66**, 1434 (1991).
- [22] J. P. Briand, P. Chevallier, P. Indelicato, K. P. Ziocck, and D. Dietrich, *Phys. Rev. Lett.* **65**, 2761 (1990).
- [23] Th. Stöhlker, P. H. Mokler, K. Beckert, F. Bosch, H. Eickhoff, B. Franzke, M. Jung, T. Kandler, O. Klepper, C. Kozhuharov, R. Moshhammer, F. Nolden, H. Reich, P. Rymuza, P. Spädtke, and M. Steck, *Phys. Rev. Lett.* **71**, 2184 (1993).
- [24] J. H. Lupton, D. D. Dietrich, C. J. Hailey, R. E. Stewart, and K. P. Ziocck, *Phys. Rev. A* **50**, 2150 (1994).
- [25] P. Beiersdorfer, D. Knapp, R. E. Marrs, S. R. Elliott, and M. H. Chen, *Phys. Rev. Lett.* **71**, 3939 (1993).
- [26] P. Beiersdorfer, *Nucl. Instrum. Methods Phys. Res. B* **99**, 114 (1995).
- [27] D. A. Knapp, R. E. Marrs, S. R. Elliott, E. W. Magee, and R. Zasadzinski, *Nucl. Instrum. Methods A* **334**, 305 (1993).
- [28] R. E. Marrs, S. E. Elliott, and D. A. Knapp, *Phys. Rev. Lett.* **72**, 4082 (1994).
- [29] S. Martin, J. P. Buchet, M. C. Buchet-Poulizac, A. Denis, J. Desesquelles, M. Druetta, J. P. Grandin, D. Hennecart, X. Husson, and D. Lecler, *Europhys. Lett.* **10**, 645 (1989).
- [30] U. Feldman, J. O. Eckberg, J. F. Seely, C. M. Brown, D. R. Kania, B. J. MacGowan, C. J. Keane, and W. E. Behring, *J. Opt. Soc. Am. B* **8**, 531 (1991).
- [31] P. Beiersdorfer, M. Bitter, S. von Goeler, S. Cohen, K. W. Hill, J. Timberlake, R. S. Walling, M. H. Chen, P. L. Hagelstein, and J. H. Scofield, *Phys. Rev. A* **34**, 1297 (1986).
- [32] P. Beiersdorfer, S. von Goeler, M. Bitter, E. Hinnov, R. Bell, S. Bernabei, J. Felt, K. W. Hill, R. Hulse, J. Stevens, S. Suckewer, J. Timberlake, A. Wouters, M. H. Chen, J. H. Scofield, D. D. Dietrich, M. Gerassimenko, E. Silver, R. S. Walling, and P. L. Hagelstein, *Phys. Rev. A* **37**, 4153 (1988).
- [33] P. Beiersdorfer, M. H. Chen, R. E. Marrs, and M. A. Levine, *Phys. Rev. A* **41**, 3453 (1990).
- [34] A. Bar-Shalom, M. Klapisch, and J. Oreg, *Phys. Rev. A* **38**, 1773 (1988).
- [35] I. G. Brown, J. E. Galvin, R. A. MacGill, and R. T. Wright, *Appl. Phys. Lett.* **49**, 1019 (1986).
- [36] W. Lotz, *Z. Phys.* **216**, 241 (1968).
- [37] Y. S. Kim and R. H. Pratt, *Phys. Rev. A* **27**, 2913 (1983).
- [38] P. Beiersdorfer, R. E. Marrs, J. R. Henderson, D. A. Knapp, M. A. Levine, D. B. Platt, M. B. Schneider, D. A. Vogel, and K. L. Wong, *Rev. Sci. Instrum.* **61**, 2338 (1990).
- [39] P. Beiersdorfer, V. Decaux, S. Elliott, K. Widmann, and K. Wong, *Rev. Sci. Instrum.* **66**, 303 (1995).
- [40] K. Wong, P. Beiersdorfer, R. E. Marrs, B. M. Penetrante, K. J. Reed, J. H. Scofield, D. A. Vogel, and R. Zasadzinski, *Nucl. Instrum. Methods B* **72**, 234 (1992).
- [41] J. D. Garcia and J. E. Mack, *J. Opt. Soc. Am.* **55**, 654 (1965).
- [42] G. W. Erickson, *J. Phys. Chem. Ref. Data* **6**, 831 (1977).
- [43] W. R. Johnson and G. Soff, *At. Data Nucl. Data Tables* **33**, 405 (1985).
- [44] J. P. Briand, J. P. Mossé, P. Indelicato, P. Chevallier, D. Girard-Vernhet, and A. Chetoui, *Phys. Rev. A* **28**, 1413 (1983).
- [45] H. F. Beyer, R. D. Deslattes, F. Folkmann, and R. E. Villa, *J. Phys. B* **18**, 207 (1985).
- [46] E. S. Marmor, J. E. Rice, E. Källne, J. Källne, and R. E. LaVilla, *Phys. Rev. A* **33**, 774 (1986).
- [47] E. R. Cohen and B. N. Taylor, *Rev. Mod. Phys.* **59**, 1121 (1987).
- [48] I. C. Percival and M. J. Seaton, *Philos. Trans. R. Soc. London A* **251**, 113 (1958).
- [49] U. Fano and J. H. Macek, *Rev. Mod. Phys.* **45**, 553 (1973).
- [50] J. R. Henderson, P. Beiersdorfer, C. L. Bennett, S. Chantrenne, D. A. Knapp, R. E. Marrs, M. B. Schneider, K. L. Wong, G. A. Doschek, J. F. Seely, C. M. Brown, R. E. LaVilla, J. Dubau, and M. A. Levine, *Phys. Rev. Lett.* **65**, 705 (1990).
- [51] H. L. Zhang, D. H. Sampson, and R. E. H. Clark, *Phys. Rev. A* **41**, 198 (1990).
- [52] K. J. Reed and M. H. Chen, *Phys. Rev. A* **48**, 3644 (1993).
- [53] P. Beiersdorfer, T. W. Phillips, K. L. Wong, R. E. Marrs, and D. A. Vogel, *Phys. Rev. A* **46**, 3812 (1992).
- [54] J. H. Scofield, *Phys. Rev. A* **44**, 139 (1991).
- [55] D. Vogel, P. Beiersdorfer, V. Decaux, and K. Widmann, *Rev. Sci. Instrum.* **66**, 776 (1995).
- [56] J. F. Seely and U. Feldman, *Phys. Rev. Lett.* **54**, 1016 (1985).
- [57] W. C. Martin, *Phys. Scripta* **24**, 725 (1989).
- [58] G. W. F. Drake, *Can. J. Phys.* **66**, 586 (1988).
- [59] D. R. Plante, W. R. Johnson, and J. Sapirstein, *Phys. Rev. A* **49**, 3519 (1994).
- [60] K. T. Cheng, M. H. Chen, W. R. Johnson, and J. Sapirstein, *Phys. Rev. A* **50**, 247 (1994).
- [61] Y.-K. Kim, D. H. Baik, P. Indelicato, and J. P. Desclaux, *Phys. Rev. A* **44**, 148 (1991).
- [62] P. Indelicato and J. P. Desclaux, *Phys. Rev. A* **42**, 5139 (1990).
- [63] B. Edlén, *Phys. Scr.* **28**, 51 (1983).
- [64] E. Hinnov and the TFTR Operating Team, and B. Denne and the JET Operating Team, *Phys. Rev. A* **40**, 4357 (1989).
- [65] G. Plunien, B. Müller, W. Greiner, and G. Soff, *Phys. Rev. A* **43**, 5853 (1991).
- [66] M. H. Chen, K. T. Cheng, W. R. Johnson, and J. Sapirstein, *Phys. Rev. A* **52**, 266 (1995).
- [67] J. P. Desclaux, in *Atomic Theory Workshop on Relativistic and QED Effects in Heavy Atoms*, edited by H. P. Kelly and Y.-K. Kim, AIP Conf. Proc. No. 136 (AIP, New York, 1985).
- [68] I. P. Grant, B. J. McKenzie, P. H. Norrington, D. F. Mayers, and N. C. Pyper, *Comput. Phys. Commun.* **21**, 207 (1980).
- [69] K. G. Dyall, I. P. Grant, C. T. Johnson, F. A. Parpia, and E. P. Plummer, *Comput. Phys. Commun.* **55**, 425 (1989).
- [70] M. H. Chen, K. T. Cheng, W. R. Johnson, and J. Sapirstein, *Bull. Am. Phys. Soc.* **39**, 1182 (1994).